PROCEEDINGS OF SCIENCE

Variations in the dip properties of XB 1254-69 observed with XMM-Newton and INTEGRAL

María Díaz Trigo*
XMM-Newton Science Operations Centre, ESAC, ESA
E-mail: mdiaz@sciops.esa.int

Arvind Parmar
Astrophysics Mission Division, Research and Scientific Support Department, ESTEC, ESA

Laurence Boirin and Christian Motch
Observatoire Astronomique de Strasbourg, France

Antonio Talavera
XMM-Newton Science Operations Centre, ESAC, ESA

Solen Balman
Middle East Technical University, Ankara, Turkey

We have analysed data from five XMM-Newton observations of XB 1254−690, one of them simultaneous with INTEGRAL, to investigate the mechanism responsible for the highly variable dips durations and depths seen from this low-mass X-ray binary. Deep dips were present during two observations, shallow dips during one and no dips were detected during the remaining two observations. The folded V-band Optical Monitor light curves obtained when the source was undergoing deep, shallow and no detectable dipping exhibit sinusoid-like variations with different amplitudes and phases. We fit EPIC spectra obtained from "persistent" or dip-free intervals with a model consisting of disc-blackbody and thermal comptonisation components together with Gaussian emission features at 1 and 6.6 keV modified by absorption due to cold and photo-ionised material. None of the spectral parameters appears to be strongly correlated with the dip depth except for the temperature of the disc blackbody which is coolest (kT$\sim$1.8 keV) when deep dips are present and warmest (kT$\sim$2.1 keV) when no dips are detectable. We propose that the changes in both disc temperature and optical modulation could be explained by the presence of a tilted accretion disc in the system.

VII Microquasar Workshop: Microquasars and Beyond
September 1 - 5, 2008
Foca, Izmir, Turkey

*Speaker.

PoS(MQW7)058

1. Introduction

Around 10 galactic low-mass X-ray binaries (LMXBs) exhibit periodic dips in their X-ray intensity. The dips are believed to be caused by periodic obscuration of the central X-ray source by structure located in the outer regions of a disc [17]. The depth, duration and spectral evolution of the dips varies from source to source and often from cycle to cycle. The 1–10 keV spectra of most of the dip sources become harder during dipping. However, these changes are inconsistent with a simple increase in photo-electric absorption by cool material, as an excess of low-energy photons is usually present. Narrow absorption features from highly ionised Fe and other metals have been observed from a number of dipping LMXBs and microquasars (e.g. [12,15]). The important role that photo-ionised plasmas play in LMXBs was recognised by [5] and [7] who were able to model the changes in *both* the narrow X-ray absorption features and the continuum during the dips from all the bright dipping LMXB observed by XMM-Newton by an increase in the column density and a decrease in the amount of ionisation of a photo-ionised absorbing plasma. Since dipping sources are normal LMXBs viewed from close to the orbital plane, this implies that photo-ionised plasmas are common features of LMXBs. Outside of the dips, the properties of the absorbers do not vary strongly with orbital phase suggesting that the ionised plasma has a cylindrical geometry with a maximum column density close to the plane of the accretion disc.

Dipping activity from XB 1254−690 was discovered during EXOSAT observations in 1984 when the source exhibited irregular reductions in X-ray intensity that repeated every 3.88 ± 0.15 hr [6]. In a 1984 August observation, five deep dips were observed with a mean duration of $\sim$0.8 hr and reduction in 1–10 keV intensity of $\sim$95%. V-band observations of the 19th magnitude companion revealed an optical modulation with minima occurring $\sim$0.2 cycles after the X-ray dips [11]. The optical modulation has a period of 3.9334 ± 0.0002 hr, consistent with the mean X-ray dip recurrence interval, and can be modelled as resulting primarily from viewing different aspects of the X-ray heated atmosphere of the companion star with a small contribution from the bulge where the accretion stream impacts the outer disc [11]. This indicates that the accretion disc does not entirely shadow the companion. The presence of dips and the lack of X-ray eclipses provides a constraint on the inclination angle, i, of the source of between 65° and 73° [6,11].

Deep dips were present during a *Ginga* observation of XB 1254−690 in 1990 [16], but were not detected during RXTE observations in 1997 [13] and *BeppoSAX* observations in 1998 [9]. Optical observations in 1997 revealed that the mean V magnitude was unchanged, but that the amplitude of the optical variability had declined by ΔV $\sim$0.1 mag [13]. This may be explained if the vertical structure at the outer regions of the disc responsible for the dips decreased in angular size from 17°–25° to $<$10° [13]. The dips had re-appeared during XMM-Newton and RXTE observations in 2001 January and May, but were not present during observations in 2001 December [14], 2002 February [4] and 2003 October [10]. Deep dipping had returned in an RXTE observation in 2004 May [2]. While all the well studied LMXB dippers show variability from cycle to cycle, the large variations in dip depth observed from XB 1254−690 are unusual.

The goal of this work is to investigate and explain the mechanism presumed responsible for the large changes in dip depth.

Obs Num	Observation ID	Observation Times (UTC) Start (year month day)	(hr:mn)	End (hr:mn)	Dip Depth	T (ks)
1	0060740101	2001 January 22	15:49	20:03	Deep	15.0
2	0060740901	2002 February 7	17:32	25:08	Undetected	26.8
3	0405510301	2006 September 12	16:15	08:01	Undetected	56.0
4	0405510401	2007 January 14	01:13	18:20	Deep	60.8
5	0405510501	2007 March 9	04:03	20:44	Shallow	59.2

Table 1: XMM-Newton observations of XB 1254−690. T is the total EPIC pn exposure time. Obs 4 was simultaneous with INTEGRAL.

2. Observations

We observed XB 1254−690 three times with XMM-Newton during 2006 and 2007. The second of these new observations was simultaneous with an INTEGRAL observation, which was used to extend the analysis to higher energies. In addition we re-analysed two earlier XMM-Newton observations reproted in [4] and [7]. Table 2 is a summary of the XMM-Newton observations. We used the EPIC pn in Timing Mode with the Thin filter. Only single and double events (patterns 0 to 4) were selected and source events were extracted from a $53''$ wide column centred on the source position. Background events were obtained from a column of the same width, but positioned away from the source. The Optical Monitor (OM) was operated in Image+Fast Mode in Obs 3–5. The V filter, very close to the standard Johnson V band, was used. We extracted light curves of XB 1254−690 from the high time resolution Fast Mode data with a time sampling of 100 s in the curve extraction to improve the signal-to-noise ratio. We corrected the OM Fast Window light curves and EPIC pn event times to the solar system barycentre. For the INTEGRAL observation, the standard 5 x 5 dither patterns of pointings centred on the target position were performed.

2.1 X-ray and optical light curves

Figure 1 shows 0.6–10 keV EPIC pn light curves of all five XMM-Newton observations of XB 1254−690 with a binning of 120 s. The plots have been grouped so that the upper panels show the two observations where dipping was not detected (Obs 2 and 3), the middle panels the observation where shallow dipping was detected (Obs 5), and the lower panels the two observations with deep dipping (Obs 1 and 4). "Deep" is defined as a reduction of the 0.6–10 keV flux of $\sim$10–90% when integrated over 1 hr around the dip centre compared to the flux within 1 hr measured 2 hours away from the dip centre, "Shallow" is a similar reduction of $\sim$5–10% and "Undetected" implies a reduction of $\lesssim$5%. The thick vertical tick marks indicate the expected dips times derived using the reference epoch of JD 2,454,114.65502 and a folding period of 0.163890 ± 0.000009 day [11]. The reference epoch corresponds to the centre of the first X-ray dip in Obs 4 and was determined by folding the 0.6–10 keV EPIC pn light curve of Obs 4 with the source period and fitting the resultant deep dip with a negative Gaussian function.

We extracted light curves from the V filter OM Fast Window exposures performed in Obs 3–5. The OM was not operated during Obs 1 and 2. The light curves show a sinusoid-like modulation consistent with the period of the binary. However, at a similar time resolution as the X–ray light

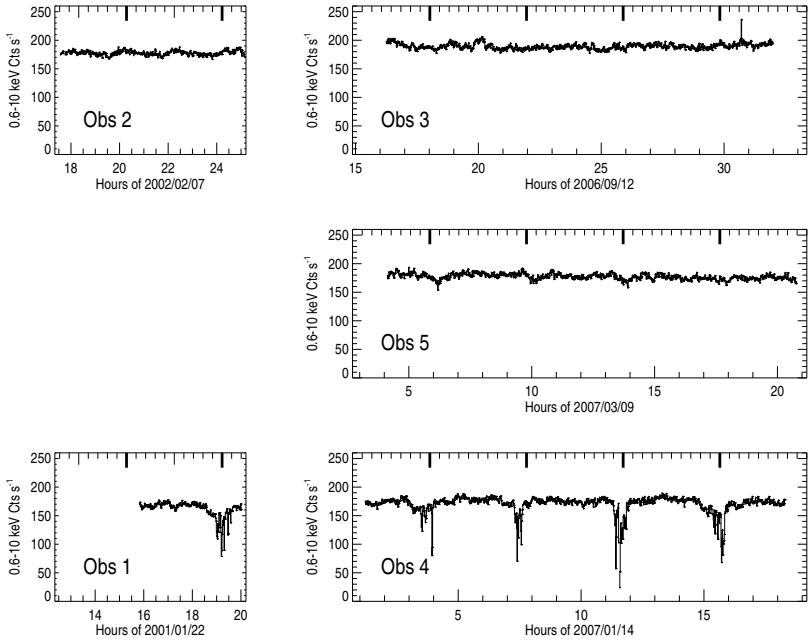

Figure 1: 0.6–10 keV EPIC pn background subtracted light curves for each XB 1254−690 observation with a binning of 120 s. The axes scales are the same for all observations. The thick vertical tick marks indicate the expected dip centres using the period of optical variations given in [11] and using the deep dips in Obs 4 to define the dip phase (see text).

curve in Fig. 1, the uncertainties on the OM lightcurves are too large to reveal details of the modulation. Thus, we resampled the light curves at 1416 s (one tenth of the binary period) and folded the light curves using the ephemeris presented earlier and examined each observation separately.

The folded light curves reveal differences in shape and magnitude between the three observations. Figure 2 shows V filter OM (lower panels) and simultaneous 0.6–10 keV EPIC pn (upper panels) light curves of XB 1254−690 folded on the orbital period, where $\phi = 0$ corresponds to optical minimum. We used the same ephemeris to fold all 3 observations. The Obs 3 OM light curve shows evidence for a secondary minimum at $\phi \sim 0.5$ which may also be present in Obs 4 as an apparent flattening of the curve around this phase, but is clearly absent in Obs 5. The average EPIC pn count rate decreased from Obs 3 to Obs 5. Finally, the phases of both the optical and X-ray modulations changed between the observations. In X-rays, we observe that the shallow dips in Obs 5 appear $\sim$0.1 later in phase compared to the deep dips in Obs 4. This difference is unlikely to be due to uncertainties in the ephemeris and the period propagation since the accumulated uncertainty from Obs 4 to Obs 5 is estimated to be $\phi < 0.0005$. Similarly, while the optical minimum falls near $\phi = 0$ for both Obs 3 and 5, it occurs later at $\phi = 0.1$ for Obs 4, when deep dips are present. We modelled the OM folded light curves with a sinusoid with the period fixed at the orbital value. This model fits well the folded light curves of Obs 4 and 5. The fit quality for Obs 3 is slightly worse than the others due to the possible presence of a secondary minimum at $\phi \sim 0.5$ which is not modelled. The results of the fits are shown in the lower panels of Fig. 2 and given in Table 2.

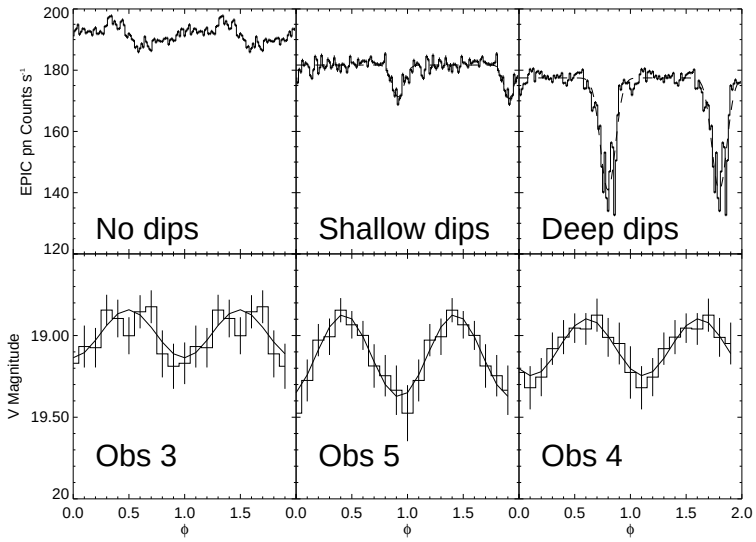

Figure 2: 0.6–10 keV EPIC pn (upper panels) and V filter OM (lower panels) XB 1254−690 light curves folded at the orbital period when no dips, shallow dips and deep dips were present. The reference epoch for phase is the same for all the plots and $\phi = 0.0$ corresponds to optical minimum. The reference phase for the optical minimum has been calculated taking into account the dip reference phase calculated in Sect. 2.1 and assuming that the dip centre occurs at $\phi = 0.8$. The binning is 1416 s and 200 s for the OM and EPIC pn light curves, respectively. The solid lines in the lower panels show the fit of Table 2.

Obs.	3	5	4
Param.			
M	18.99 ± 0.03	19.12 ± 0.03	19.07 ± 0.03
A	0.15 ± 0.04	0.25 ± 0.04	0.17 ± 0.04
ϕ_0	0.99 ± 0.04	0.93 ± 0.03	0.11 ± 0.03
χ^2_ν(d.o.f.)	0.84 (13)	0.29 (13)	0.26 (13)

Table 2: Best-fits to the folded OM light curves for Obs 3–5 using the M+A*sin(2π($c * \phi + 0.25 - \phi_0$)) model. M, A, ϕ, and ϕ_0 are the average optical magnitude, amplitude, phase and phase at the optical minimum, respectively. The coefficient c has been fixed to 1, since the curves are folded on the orbital period.

2.2 X-ray spectra

For the observations showing deep and shallow dipping, we first selected intervals of "persistent" or dip free emission. Spectra were accumulated corresponding to these intervals and for the entire dip free observations. We rebinned the EPIC pn spectra to over-sample the $FWHM$ of the energy resolution by a factor 3 and to have a minimum of 25 counts per bin, to allow the use of the χ^2 statistic. We did not rebin the JEM-X and ISGRI spectra to avoid losing spectral resolution. We performed spectral analysis using XSPEC [1] version 12.3.1. Spectral uncertainties are given at 90% confidence ($\Delta\chi^2$= 2.71 for one interesting parameter), and upper limits at 95% confidence.

Observation No.		2	3	5	1	4
Dips		Undetected	Undetected	Shallow	Deep	Deep
Parameter	Comp.					
	`comptt`					
kT_0 (keV)				0.173 ± 0.001		
$kT_{\rm comptt}$ (keV)				3.06 ± 0.03		
τ_p				6.07 ± 0.05		
$k_{\rm comptt}$		0.0747 ± 0.0005	$0.0772\ ^{+0.0003}_{-0.0015}$	$0.0763\ ^{+0.0006}_{-0.0003}$	0.0740 ± 0.0008	0.0748 ± 0.0006
	`dbb`					
$kT_{\rm bb}$ (keV)		2.128 ± 0.006	2.069 ± 0.004	1.86 ± 0.01	1.66 ± 0.01	1.74 ± 0.01
$k_{\rm bb}$ $[(R_{in}/D_{10})^2 \cos\theta]$		1.10 ± 0.01	1.363 ± 0.009	$1.76\ ^{+0.01}_{-0.03}$	2.34 ± 0.05	2.15 ± 0.04
	`gau`$_1$					
$E_{\rm gau}$ (keV)				6.59 ± 0.05		
σ (keV)				0.53 ± 0.06		
$k_{\rm gau}$ (10^{-4} ph cm^{-2} s^{-1})				3.3 ± 0.3		
	`gau`$_2$					
$E_{\rm gau}$ (keV)				1.046 ± 0.004		
σ (keV)				0.1		
$k_{\rm gau}$ (10^{-3} ph cm^{-2} s^{-1})				$1.69\ ^{+0.04}_{-0.07}$		
	`tbabs`					
$N_{\rm H}^{\rm abs}$ (10^{22} cm^{-2})		$0.225\ ^{+0.007}_{-0.004}$	0.220 ± 0.001	0.220 ± 0.001	$0.225\ ^{+0.007}_{-0.004}$	0.220 ± 0.001
	`warmabs`					
$N_{\rm H}^{\rm warmabs}$ (10^{22} cm^{-2})		2.2 ± 0.4	2.3 ± 0.3	2.0 ± 0.3	2.8 ± 0.5	2.6 ± 0.3
$\log(\xi)$ (erg cm s^{-1})		3.95 (f)	3.95 (f)	3.95 (f)	3.95 (f)	3.95 (f)
$\sigma_{\rm v}$ (km s^{-1})		$4400\ ^{+2300}_{-1900}$	3650 ± 1000	$2600\ ^{+1700}_{-1300}$	$4400\ ^{+3100}_{-1900}$	$1500\ ^{+700}_{-600}$
v (km s^{-1})		-240 $\pm$ 1200	-2040 $\pm$ 600	-1440 $\pm$ 780	$240\ ^{+1500}_{-900}$	-1380 $\pm$ 360
χ^2_ν(d.o.f.)				1.51 (1147)		
F (10^{-10} erg cm^{-2} s^{-1})		8.9	9.5	8.8	8.0	8.4

Table 3: Best-fits to the 0.6–10 keV EPIC pn, 5–25 keV JEM-X and 15–70 keV ISGRI persistent (non-dip) spectra for all the observations using the `tbabs*warmabs*(dbb+comptt)+ tbabs*(gau`$_1$`+gau`$_2$`)` `model`. $k_{\rm comptt}$, $k_{\rm bb}$ and $k_{\rm gau}$ are the normalisations of the comptonisation component, disc blackbody and Gaussian emission features, respectively. kT_0 is the input soft photon (Wien) temperature, $kT_{\rm comptt}$ the plasma temperature, and τ_p the plasma optical depth, of the comptonisation component. $kT_{\rm bb}$ is the temperature of the disc blackbody. $E_{\rm gau}$ and σ represent the energy and width of the Gaussian features. $N_{\rm H}^{\rm abs}$ and $N_{\rm H}^{\rm warmabs}$ are the column densities for the neutral and ionised absorbers, respectively. ξ, $\sigma_{\rm v}$, and v are the ionisation parameter, the turbulent velocity broadening, and the average systematic velocity shift of the absorber (negative values indicate blueshifts). F is the unabsorbed 0.6–10 keV total flux. The widths (σ) of the Gaussian emission lines `gau`$_{1-2}$ are constrained to be $\leq$1 keV and $\leq$0.1 keV, respectively. $N_{\rm H}^{\rm abs}$ is linked for Obs 1–2 and for Obs 3–5 during the fits.

We fit the 0.6–10 keV EPIC pn, 5–25 keV JEM-X and 15–70 keV ISGRI spectra of XB 1254−690 with a model consisting of a disc blackbody and a thermal comptonisation model, `comptt`, both modified by photo-electric absorption from neutral and ionised material together with two Gaussian emission features at ∼1.0 keV and ∼6.6 keV modified by neutral absorption only and one Gaussian absorption feature at ∼1.8 keV (`tbabs*warmabs*(diskbb+comptt) + tbabs*(gau+gau)` `+gau`). The feature at 1.8 keV is probably due to an incorrect modeling of the Si absorption in the CCD detectors by the EPIC pn calibration and is therefore not further discussed. The `warmabs`

component models the absorption due to a photo-ionised plasma in the line of sight and is necessary to account for the complex residuals evident near 7 keV as well as for modifying the overall continuum shape.

After performing fits for all the observations, it was evident that the disc-blackbody component was changing significantly among observations while the thermal comptonisation component was unchanged within the uncertainties. Therefore, we fit the spectra for all observations together tying the parameters of the thermal comptonisation, except the normalisation factor, and Gaussian components for all the observations. We kept the normalisation factor of the comptonisation component untied to prevent an artificial variation of the disc-blackbody flux due to the constancy of the former component. When fitting the `warmabs` component, we first searched for the lowest possible value of the ionisation parameter, ξ, which fits well the absorption lines, and then we fixed the parameter to this value to obtain the final fits and the uncertainties. This is done to prevent a fit with "artificially" increased continuum normalisations and unrealistic column densities for the absorber. The χ^2_ν of the resulting fit is 1.51 for 1147 degrees of freedom (d.o.f.). The parameters of the best-fit model are given in Table 3 and the residuals of the fit are shown in Fig. 3.

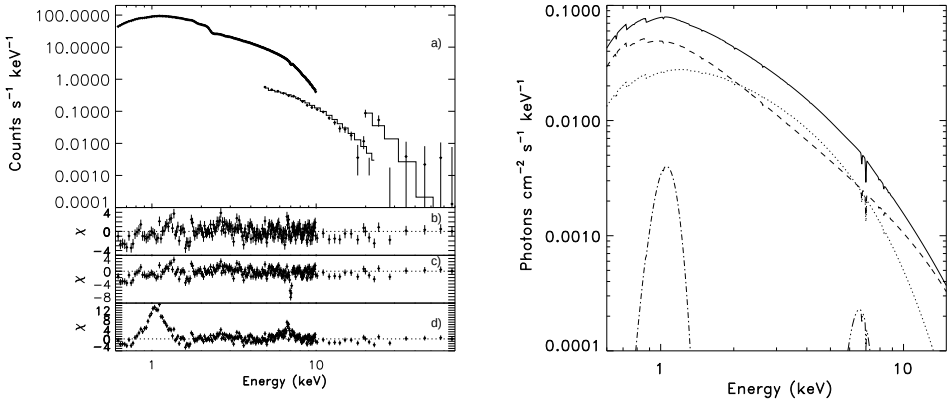

Figure 3: *Left*: 0.6–10 keV EPIC pn, 5–25 keV JEM-X and 15–70 keV ISGRI XB 1254−690 Obs 4 spectra fit with a disc-blackbody (`diskbb`) and a thermal comptonisation component (`comptt`) as continuum modified by absorption from neutral (`tbabs`) and ionised (`warmabs`) material together with two Gaussian emission lines ($\texttt{gau}_{1-2}$) which are modified by absorption from neutral material (`tbabs`) only. (b) Residuals in units of standard deviation from the above model. (c) Residuals when $N_{\rm H}^{\rm warmabs}$ is set to 0 showing the $\sim$7 keV absorption features clearly. (d) Residuals when the normalisations of the Gaussian emission lines are set to 0. Best-fit parameters are given in Table 3. *Right*: Best-fit model. Solid, dashed, dotted, dashed-dotted and dashed-dotted-dotted lines represent, respectively, the total model, the comptonisation component, the disc-blackbody component and the Gaussian features at 1 and 6.6 keV.

3. Discussion

We have analysed five XMM-Newton observations of the LMXB XB 1254−690. The 0.6–10 keV EPIC pn lightcurves are highly variable with two observations showing deep dips, one showing shallow dips and two without evidence for dipping behaviour. The X-ray continua of the dip-free intervals are well fit by a model consisting of a disc-blackbody with a thermal comptonisation component extending to higher energies. Both components are absorbed by neutral and ionised

material. The temperature of the disc blackbody is lower for observations with deep dips (1.66 ± 0.01 and 1.74 ± 0.01 keV), increases for the observations with shallow dips (1.86 ± 0.01 keV) and is highest for the observations where dips are absent (2.128 ± 0.006 and 2.069 ± 0.004 keV). We did not find any significant changes in the ionisation parameter of the absorber between the persistent emission from the different observations. However, the absorber is very strongly ionised and only features from H-like FeXXVI are evident, making it more difficult to detect ionisation changes compared to a less ionised plasma where spectral features from a range of ions are visible. A moderately broad (σ = 0.5 keV) Fe emission line at 6.6 keV with $EW \sim$50 eV and an emission line at 1 keV with $EW \sim$12 eV, are present in the spectra. The feature at 1 keV is detected in a number of X-ray binaries and has been previously modelled either as an emission line, or as an edge, and its nature is unclear (e.g., [5,7,12]). Provided the feature has an astrophysical origin, its appearance always at similar energy points to line emission, since a soft component due to a e.g. blackbody emission is expected to change its temperature for different sources. Its energy is consistent with a blend of NeIX and NeX emission, or Fe L emission. Recently, broad skewed Fe K emission lines have been discovered from a LMXB containing a neutron star (e.g. [3]). The emission feature detected in the XB 1254−690 XMM-Newton observations at 6.6 keV is weak and moderately broad. It is not necessary to invoke relativistic effects to explain the moderate line width, which could be due to mechanisms such as Compton broadening. The line is broader and has a larger equivalent width when the disc-blackbody continuum component is substituted by a blackbody. However, the fit quality is worse and the line is unrealistically large. Due to the availability of XMM-Newton and INTEGRAL simultaneous data, we are able to accurately determine the broad band continuum shape and thus we find no evidence for a relativistically broadened Fe line in XB 1254−690.

3.1 Light curve modelling

We have produced simultaneous folded optical and X-ray light curves of the three long observations which cover, shallow, deep and dip free intervals. The folded OM light curve for Obs 3 is similar to those obtained by [13]. We find the same optical average magnitude, V=19.0, and amplitude, ΔV = 0.3, as in the 1997 optical observations. Both in the 1997 RXTE observation and in Obs 3 X-ray dips are absent. In Obs 4, the folded lightcurves are very similar to the February 1984 observations shown in [6]. They report an average magnitude V = 19.0 and ΔV = 0.4 for the optical modulation. However, we extrapolate from their Fig. 3 an average magnitude of V = 19.1. These values are consistent with those shown in Table 2 for Obs 4. Finally, whilst the RXTE light curve from [2] shows one deep dip, the shape of the simultaneous optical curve seems to be more similar to that of XMM-Newton Obs 5. Unfortunately, Fig. 3 of [2] is in units of flux density rather than magnitude and we cannot easily compare their results with our fits. However, we note that the optical curve from [2] covers several cycles while only one X-ray cycle is shown. We have observed that the X-ray behaviour has changed in the cycles following the dip, so this may explain the shape and amplitude of Fig. 3 from [2].

[13] interpret the decrease in optical magnitude and the cessation of dipping activity in the August 1984 to the 1997 observations as an indication of a decrease in the bulge size, implying that the bulge contributes $\sim$35–40% to the optical modulation. In contrast, [11] interpreted the shape and phase of the optical modulation as indicating that the majority of the optical modulation is caused by viewing varying aspects of the X-ray heated hemisphere of the companion star with

the contribution of the material responsible for the X-ray dips being responsible of $<$15% of the disc emission. The XMM-Newton OM light curves show an optical modulation which is $\sim$20% of the disc emission, implying that the results of [13] and [11] are in disagreement. In the first interpretation, the majority of the steady component from the optical flux comes from the disc. During dipping intervals, cooler material at the disc rim could obscure part of the hotter, inner disc regions. The disappearance or reduction in size of the azimuthal structure could lead to a more direct viewing of the hot inner disc regions and an increase in the apparent mean disc emission temperature. This interpretation explains naturally the increase in the temperature of the disc with decreasing dip depth that we observe. However, following this we should observe the $\sim$35–40% bulge contribution to the optical modulation mainly at $\phi = 0.8$, when the X-ray dips are observed, and even a higher contribution at $\phi = 0.3$, since the inner bulge should be brighter. Clearly, though we see a significant excess of optical emission at $\phi = 0.8$ during deep dipping observations, compared to persistent and shallow dipping observations, we do not see such excess at $\phi = 0.3$, and the fact that the optical minimum is observed at $\phi \sim 0$ is in favour of the optical modulation being caused by the heated hemisphere of the companion.

3.2 Explanation for the changes in optical and X-ray emission

We propose that the modulation of the optical light curves is due primarily to obscuration by a precessing accretion disc that is tilted out of the orbital plane. The model is similar to that proposed by [8] for Her X-1, and explains naturally the appearance and disappearance of dips observed in the X-ray emission of XB 1254−690, as well as the spectral changes in the continuum seen in different observations. In such a model, the accretion disc performs three major roles in the optical flux variations: the manner in which the disc's X-ray shadow cyclically changes the illumination of the stellar companion, the periodic occultation of the companion by the disc, and the changing optical brightness of the disc itself due to the changing aspect. It is this varying aspect which may cause the changes observed in X-ray luminosity and disc temperature and in addition the periodic appearance and disappearance of dips in XB 1254−690 due to its particular inclination with respect to the observer, $\sim 70^{\circ}$.

A qualitative explanation of the model comes from the schematic precessing disc model shown in Fig. 3 by [8]. In all cases, the main contribution to the optical flux is due to the X-ray reprocessed emission from the disc, represented in the model that fits the OM light curves by the average magnitude M. The angle from which the observer views the pattern of re-emitted light from the disc gradually changes through the precession cycle. A second contribution to the optical flux arises from the heated face of the companion. A maximum contribution of optical light is expected when the observer sees the part of the star facing the disc, $\phi = 0.5$, and a minimum when the heated face is out of view, at $\phi = 0.0$. This component is represented in our model by the sine component. A secondary minimum in the optical light curve is due to the shadowing by the disc of the heated face at $\phi = 0.5$. Depending on the orientation of the disc with respect to the star, such minima could be prominent, as in Obs 3, or almost invisible, as in Obs 5. This secondary minimum is also visible in the average light curve in [11].

In XB 1254−690, dipping should preferentially occur when the inclination of the disc on the line of sight is highest. The disc inclination is never large enough to produce total eclipses, but at orbital phase $\sim$ 0.8, the bulge, assumed to be fixed in phase on the disc edge, can partially block

the view to the neutron star at some precessional phases. In the case of Her X-1, dipping episodes would correspond to the short "on" state occurring between phases 0.4 and 0.65 in the ephemeris of [8]. For this particular disc orientation, the 1.7 d light curve of Her X-1 displays a shoulder at orbital phase $\sim$0.8 similar to that observed in XB 1254$-$690. This additional light component is probably due to the X-ray heated stellar region whose centroid is facing the observer, an area unshielded by the disc in this particular geometrical observer-disc configuration. Because of the varying height of the bulge, the appearance of X-ray dips may not necessarily follow a strictly period pattern. This possibly accounts for the fast dip to no dip regime change sometimes observed (e.g. [6]). Non dipping episodes should coincide with low disc inclinations which in the light curve of Her X-1 correspond to precession phases $\sim$0 [8]. At these precessional phase, the disc casts a maximum shadow on the secondary star at inferior conjunction thus producing a secondary minimum at orbital phase 0.5 in Her X-1, similar to that seen in the light curve of Obs 3. Finally, shallow dipping would occur at an intermediate configuration between the deep dipping and the non dipping conditions, when the the bulge is observed at grazing angles due to its varying height.

Although disc precession can qualitatively explain the appearance and disappearance of X-ray dips as well as the gross features of the optical light curve, we stress that such an explanation remains unproven in the absence of detailed light curve modelling. In particular, the compatibility of the disc opening angle, bulge height and possible tilt angles with the observed light curve cannot be ascertained.

References

[1] Arnaud, K. A. 1996, in ASP Conf. Ser. 101: Astronomical Data Analysis Software and Systems V, 17

[2] Barnes, A. D., Casares, J., Cornelisse, R., et al. 2007, MNRAS, 380, 1182

[3] Bhattacharyya, S. & Strohmayer, T. 2007, ApJ, 664, 103B

[4] Boirin, L. & Parmar, A. N. 2003 A&A, 407, 1079

[5] Boirin, L., Méndez, M., Díaz Trigo, M., Parmar, A. & Kaastra, J.: 2005, A&A 436, 195

[6] Courvoisier, T. J. L., Parmar, A. N., Peacock, A., & Pakull, M. 1986, ApJ, 309, 265

[7] Díaz Trigo, M., Parmar, A., Boirin, L., Méndez, M. & Kaastra, J.: 2006a, A&A 445, 179

[8] Gerend, D. & Boynton, P. E. 1976, ApJ, 209,562

[9] Iaria, R., di Salvo, Burderi, L., & Robba, N. R. 2001 , ApJ, 584, 883

[10] Iaria, R., di Salvo, T., Lavagetto, G., D'Aí, A., & Robba, N. R. 2007, A&A, 464, 291

[11] Motch, C., Pedersen, H., Courvoisier, T. J. L., Beuermann, K., & Pakull, M. W. 1987, ApJ, 313, 792

[12] Sidoli, L., Oosterbroek, T., Parmar, A. N., Lumb, D., & Erd, C. 2001, A&A, 379, 540

[13] Smale, A. P. & Watcher, S. 1999, ApJ, 527, 341

[14] Smale, A. P., Church, M. J. & Balucinska-Church, M. 2002, ApJ, 581, 1286

[15] Ueda,Y., Inoue, H., Tanaka, Y., et al. 1998, ApJ 492, 782

[16] Uno, S. Mitsuda, K., Aoki, T., & Makino, F. 1997, PASJ, 49, 353

[17] White, N. E. & Swank, J. H. 1982, ApJ, 253, L61